

PSFC/JA-04-45

**Active and Fast Particle Driven Alfvén Eigenmodes
in Alcator C-Mod**

J.A. Snipes, N. Basse, C. Boswell, E. Edlund, A. Fasoli^a, N.N.
Gorelenkov^b, R.S. Granetz, L. Lin, Y. Lin, R. Parker, M. Porkolab,
J. Sears, S. Sharapov^c, V. Tang, S. Wukitch

16 November 2004

Massachusetts Institute of Technology, Plasma Science and Fusion Center
Cambridge, MA 02139 USA

^a Centre de Recherches en Physique des Plasmas, Association Euratom—Confédération
Suisse, Ecole Polytechnique Fédérale de Lausanne, CH-1015 Lausanne, Switzerland

^b Princeton Plasma Physics Laboratory, Princeton, NJ USA 08543

^c Euratom/United Kingdom Atomic Energy Authority Fusion Association,
Culham Science Centre, Abingdon, OX14 3DB, UK

This work was supported by the U.S. Department of Energy, Cooperative Grant No.
DE-FC02-99ER54512. Reproduction, translation, publication, use and disposal, in whole
or in part, by or for the United States government is permitted.

Submitted for publication to *Physics of Plasma*.

Active and fast particle driven Alfvén eigenmodes in Alcator C-Mod

J A Snipes,^{a)} N Basse, C Boswell, E Edlund, A Fasoli,^{b)} N N Gorelenkov,^{c)}
R S Granetz, L Lin, Y Lin, R Parker, M Porkolab, J Sears,
S Sharapov,^{d)} V Tang, S Wukitch

^{a)} *Electronic mail: snipes@psfc.mit.edu*

Massachusetts Institute of Technology Plasma Science and Fusion Center, Cambridge, MA USA 02139

^{b)} *Centre de Recherches en Physique des Plasmas, Association Euratom – Confédération Suisse, Ecole Polytechnique Fédérale de Lausanne, CH-1015 Lausanne, Switzerland*

^{c)} *Princeton Plasma Physics Laboratory, Princeton, NJ USA 08543*

^{d)} *Euratom/United Kingdom Atomic Energy Authority Fusion Association, Culham Science Centre, Abingdon, OX14 3DB, UK*

Abstract

Alfvén eigenmodes (AEs) are studied to assess their stability in high density reactor relevant regimes where $T_i \approx T_e$ and as a diagnostic tool. Stable AEs are excited with active MHD antennas in the range of the expected AE frequency. Toroidal Alfvén eigenmode (TAE) damping rates between $0.5\% < \gamma/\omega < 4.5\%$ have been observed in diverted and limited Ohmic plasmas. Unstable AEs are excited with a fast ion tail driven by H minority ion cyclotron radio frequency (ICRF) heating with electron densities in the range of $\bar{n}_e = 0.5 - 2 \times 10^{20} \text{ m}^{-3}$. Energetic particle modes (EPMs) or TAEs have been observed to decrease in frequency and mode number with time up to a large sawtooth collapse, indicating the role fast particles play in stabilizing sawteeth. In the current rise phase, unstable modes with frequencies that increase rapidly with time are observed with magnetic pick-up coils at the wall and Phase Contrast Imaging (PCI) density fluctuation measurements in the core. Modeling of these modes constrains the calculated safety factor profile to be very flat or with slightly reversed shear. AEs are found to be more stable for an inboard than for central or outboard ICRF resonances in qualitative agreement with modeling.

I. Introduction

Alfvén eigenmodes have been studied on a number of magnetic fusion devices since the first experimental observations on TFTR.¹⁻⁵ Calculations indicate that fusion generated α particles may destabilize these modes in next step devices such as ITER⁶ and if the modes are large enough to transport substantial amounts of hot α particles from the core of the plasma, they could quench the fusion burn or lead to damage to the first wall. The energetic ions that destabilize Alfvén eigenmodes in present devices are produced by neutral beam injection or ion cyclotron radio frequency (ICRF) heating. The growth rate of these modes depends on a balance of energetic particle drive⁷⁻⁹ with a number of possible damping mechanisms.¹⁰⁻¹²

To separate the damping from the drive, experiments have been performed on JET with low toroidal mode number, $n \leq 2$, active MHD antennas¹³⁻¹⁵ that excite stable Alfvén eigenmodes in the plasma at the expected mode frequency, which for toroidal Alfvén eigenmodes (TAEs) is given approximately by the center of the gap frequency¹⁶ $\omega_{\text{TAE}} = v_A/(2qR)$ where $v_A \propto B/(m_i n_i)^{0.5}$ is the Alfvén velocity. Here, B is the magnetic field on axis, m_i is the effective ion mass, n_i is the ion density, q is the safety factor at the resonant surface, and R is the major radius of the magnetic axis. These stable modes are excited in Ohmic plasmas in the absence of energetic particles to ensure that the energetic particle drive terms are zero in order to isolate the damping rate of the mode. On Alcator C-Mod, similar experiments have begun with moderate $|n| \leq 16$ active MHD antennas¹⁷ since moderate n are expected to be the most unstable in ITER.⁶ These modes are excited in C-Mod plasmas with the same toroidal field and density expected in ITER and with equilibrated ion and electron temperatures required for such a burning plasma.

Alfvén Eigenmodes have been observed during sawtooth stabilization in the current flattop in JT-60U,¹⁸ TFTR,¹⁹ and DIII-D.²⁰ These modes indicate the presence of fast particles that are believed to be responsible for stabilizing the sawteeth.²¹ Analysis of these experiments has shown that fast ions are expelled from within the $q=1$ radius because of these modes. This redistribution of fast ions weakens sawtooth stabilization leading to the large sawtooth collapse. Similar modes are observed during sawtooth stabilization in Alcator C-Mod even with densities up to $\bar{n}_e \approx 2 \times 10^{20} \text{ m}^{-3}$, indicating that a high energy fast ion tail is produced with sufficient ICRF heating.

With strong heating in the current rise, rapidly changing frequency Alfvén eigenmodes have been observed in a number of tokamaks²²⁻²⁵, known as Alfvén cascades. According to the Berk and Breizman theory,²⁶ the rapidly changing frequency of these modes indicates that there is a very flat or reversed shear q profile and, for fixed poloidal (m) and toroidal (n) mode numbers, the frequency should change as a function of the minimum q value:

$$\omega(t) = \left| \frac{m}{q_{\min}(t)} - n \right| \cdot \frac{v_A}{R_0} + \omega_0. \quad (1)$$

The value of the minimum frequency, ω_0 , is determined by continuum damping including pressure effects. This simple model fits the JET data very well and allows the Alfvén cascades to constrain q_{\min} . Together with calculations of the Alfvén eigenmode structure with the MISHKA code²⁷ it is then possible to model the core q profile evolution based on the Alfvén cascades. In this way, Alfvén cascades in Alcator C-Mod have been used to model the evolution of the q profile in the current rise of strongly ICRF heated discharges.

II. Stable Alfvén eigenmode experiments

To complement the previous low n experiments on JET,¹³⁻¹⁵ a pair of moderate n active MHD antennas was installed on C-Mod to excite a broad toroidal mode spectrum ($|n_{FWHM}| \sim 16$) of stable Alfvén eigenmodes and measure their damping rates at ITER toroidal fields and densities with equilibrated ion and electron temperatures.¹⁷ Each antenna has five turns each 15 cm toroidally \times 25 cm poloidally, centered about 18 cm above and below the outboard midplane. For these experiments, only the upper antenna was excited with an amplifier that coupled up to 3 kW of power at 10 A. So, the excited perturbations are so small that they do not significantly perturb the plasma and the resulting AE resonances ($\tilde{B}_\theta < 10^{-6}$ T) can only be observed with the most sensitive fluctuation diagnostics. Toroidal arrays of three magnetic pick-up coils mounted beneath the tiles 10 cm above and below the outboard midplane on each of two limiters were used to measure the AEs in the plasma through software synchronous detection with the antenna current. They can measure fluctuation levels down to about $\tilde{B}_\theta \sim 10^{-7}$ T. The data were sampled for 12 signals throughout the discharge at 2.5 MHz.

The simplest way to excite TAE resonances in the plasma is to drive the antenna at constant frequency and then sweep the density or toroidal field so that the center of the TAE gap frequency in the plasma passes through the active MHD frequency. This avoids any problems with matching to the antenna inductance or any resonance in the circuit so that even a rather weak resonance may be observed. Figure 1 shows an example where the toroidal field was ramped down and then back up so that the TAE frequency in the plasma passed through the active MHD frequency twice and two clear resonances are observed on the Fourier transform of a pick-up coil signal. The TAE resonances are

observed to coincide with the TAE frequency at the $q=1.5$ surface, as also observed in JET.⁴ This is expected theoretically, as long as the antennas couple to this resonance, since the least stable TAE is at the $q=1.5$ surface for a monotonic q profile, halfway between the $m=1$ and $m=2$ continua.²⁸

To observe multiple resonances in a single discharge and follow the resonance in time, the antenna frequency can be swept up and down through the expected TAE resonant frequency in the plasma (Figure 2). To maintain sufficient matching between the antenna and the amplifier to observe resonances, the frequency could be swept by at most ± 50 kHz. Through software synchronous detection between the antenna current and the pick-up coil signals,¹⁷ the damping rate of the mode was found to be $\gamma/\omega \sim 4.5\%$ with $n = 12$ in this case.

An experiment was performed at constant active MHD frequency ramping the toroidal field for a number of inner wall limited Ohmic discharges with different elongations to determine the dependence of the TAE damping rate on edge shear. The plasma parameters were $I_p = 0.7$ MA, $4.7 \text{ T} < B_T < 5.6 \text{ T}$, $\bar{n}_e = 2 - 2.5 \times 10^{20} \text{ m}^{-3}$, $3.1 < q_{95} < 4.5$, and $370 < f_{\text{TAE}}(q=1.5) < 470$ kHz. Figure 3 shows the measured damping rates for each discharge as a function of elongation and edge shear calculated at the 95% flux surface. In contrast to the results on JET for low n modes,¹⁴ no clear dependence on edge shear is found for these moderate n modes and the damping rate appears to decrease with increasing elongation. Note that with only a single antenna, no selection can be made for the excited mode number and the plasma responds with measured toroidal mode numbers in the range of $4 < |n| < 14$. So, it is possible that a dependence of the damping rate on mode number could mask a dependence on edge shear.

III. Alfvén eigenmodes during sawtooth stabilization

Alfvén eigenmodes are observed in C-Mod during the current flattop in the presence of sawteeth even at electron densities up to $\bar{n}_e = 2 \times 10^{20} \text{ m}^{-3}$ when there is sufficient ICRF heating. Mode frequencies corresponding to the TAE and EAE gaps associated with $q=1$ are observed with decreasing frequency as q evolves up to the sawtooth collapse.

Figure 4 shows an example of sawtooth stabilization with ICRF heating during a double null discharge. The plasma has a brief H-mode from 0.76 to 0.784 s where the central line averaged density rises from 1.6 to nearly $2 \times 10^{20} \text{ m}^{-3}$. The resulting drop in the TAE frequency is evident in the calculated center of the gap frequency for $q=1$ just before the sawtooth collapse that ends the H-mode. The modes begin with relatively high $|n| = 8 - 10$ at about 750 kHz, then coalesce as the frequency drops to 650 kHz with increasing density in the H-mode and the mode numbers also drop to $|n| = 4 - 5$ just before the sawtooth collapse. Note that since the plasma current is negative (clockwise viewed from above), these modes with negative n numbers rotate in the ion diamagnetic drift direction. The coalescing of the modes to a single frequency suggests that the AE gap is closing as the sawtooth evolves or that they reach the bottom of the gap.²⁹ One would expect that the previous sawtooth collapse flattens the core q profile producing a relatively broad TAE gap. Then, as the sawtooth heats up, the current density profile should peak with peaking temperature, which would tend to close the TAE gap until the large sawtooth collapse.

Attempts were made to model the modes with the Nova-K code³⁰ at $t=0.74$ and $t=0.78$ s. Eigenmodes were found in the same range of mode numbers and frequencies as in the experiment. The radial structure at $t=0.74$ s was that expected for TAEs with two dominant harmonics m and $m+1$ peaked at $r/a = 0.4$, while the radial structure at $t=0.78$ s had multiple poloidal harmonics between $0.4 < r/a < 0.9$. The trapped particle growth rates were found to be stable because of relatively large radiative damping even for flat shear q profiles out to $r/a = 0.4$, varying q_0 from 1 down to 0.8 and varying the assumed fast ion energy from 10 keV to 490 keV. The TRANSP calculated fast ion energy peaked at about 300 keV for these conditions. This may indicate that these are energetic particle modes (EPMs)³¹ that are not included in the Nova-K code or core localized TAEs³² with a different q profile.

IV. Alfvén cascades in the current rise

With H minority ICRF heating in the current and density rise on C-Mod, an energetic H ion tail is driven that excites rapidly increasing frequency Alfvén cascades when the minimum in the q profile is substantially greater than unity and has very flat or perhaps slightly reversed shear. Although not recognized as ACs at the time, these modes were the first Alfvén eigenmodes observed on C-Mod in the initial current rise ICRF heating experiments performed in 1996.²⁰ More recent experiments with more than twice as much ICRF power and the addition of the phase contrast imaging (PCI) diagnostic³³ have improved our understanding of these modes and the conditions that lead to them.

A. Core and edge Alfvén cascade measurements

In addition to the magnetic pick-up coils on the outboard limiters that measure the more radially extended low n Alfvén eigenmodes, the PCI diagnostic measures the density fluctuations of the AEs along 32 vertical chords passing through the plasma core. It is sensitive to major radial wavenumbers from $0.5 < k_R < 17 \text{ cm}^{-1}$ and the data are sampled at 10 MHz. The magnetic pick-up coils are sampled at 2.5 MHz and can measure toroidal mode numbers up to $n < 75$. Figure 5 shows a comparison of ACs measured with magnetic pick-up coils and with PCI. The slopes of the ACs are much higher on the PCI measurements than on the magnetic measurements. According to theory, the slopes are proportional to the n number, implying that the PCI measurements through the core are more sensitive to higher mode numbers than the edge magnetic measurements, similar to what has recently been found on JET.³⁴

The phase differences between toroidally separated pick-up coils during the ACs indicate that the dominant modes are low n , but despite detailed in-vessel calibrations of the frequency dependence of the phase differences between the coils, the n numbers appear to change during the upward sweep in frequency for some cascades. This is in contrast to the constant n observed in JET and JT-60U for each frequency sweeping mode. However, in the case of Figure 5, there are three modes visible in the magnetic spectrogram starting at about 0.12 s with slopes that are 1, 2, and 3 times the slope of the dominant mode, indicating that they correspond to $n = 1, 2, \text{ and } 3$. The PCI and magnetic measurements complement each other in that the lowest n modes are often not visible on the PCI because the sensitivity of the instrument falls off for long wavelength modes.³⁵

B. Modeling the evolution of the safety factor profile

Given the n numbers from the slopes of the ACs and the frequency evolution of the modes, the MISHKA code was used to model the evolution of the q profile. Figure 6 shows the calculated evolution of the minimum in q from the measured frequency evolution of the modes in Figure 5 together with the modeled q profile at the start of the cascades. The start of an AC with multiple modes like that at 0.12 s indicates that q_{min} is passing through an integer value and then the appearance of another $n=2$ mode at about 0.14 s indicates q_{min} is passing through the next half-integer value. Reversed shear was not required to find the modes in these calculations, but the calculated q profile was rather flat at q_{min} out to $r/a \approx 0.4$ then rose to $q_{95} \approx 5$.

During the upward frequency sweep of each mode, the calculated mode structure has a single dominant m characteristic of an AC. The continuum also has a wide gap, which allows the mode frequency to start well below the TAE frequency without being strongly damped by the continuum. Just after the frequency peaks and begins to decrease, the mode structure evolves into a TAE structure with comparable amplitudes of two poloidal harmonics m and $m+1$. The continuum gap then narrows around the TAE frequency.

C. Fast particle calculations

The TRANSP/FPPRF code³⁶ was used with TORIC³⁷ to calculate the RF electric field distribution to estimate the fast particle energy profile. Figure 7 shows the calculated time evolution of the fast hydrogen ion energy together with its radial profile and the RF power deposition during the TAEs of Figure 5. Under these relatively low density conditions with $\bar{n}_e = 1.7 \times 10^{20} \text{ m}^{-3}$, the calculated fast ion energy can exceed

300 keV with peaked RF power densities of 75 W/cm^3 . For comparison, the Stix effective temperature³⁸ for these conditions ($T_e = 3200 \text{ eV}$, $n_H/n_e \approx 0.04$) reaches almost 1 MeV. So, for these high power densities, 300 keV may be a reasonable estimate of the fast ion energy, but there are large uncertainties in the energy because of the uncertainty in the core fast ion concentration, which is based on a spectroscopic measurement of the ratio of H_α/D_α in the plasma edge. Similar results were obtained for the sawtooth stabilization case shown in Figure 4 with fast ion energies exceeding 300 keV during the modes.

D. Current rise high frequency modes above the TAE gap

In addition to Alfvén eigenmodes with frequencies below the TAE gap, there are also eigenmodes in the current rise with twice the Alfvén cascade frequencies and twice the TAE frequencies. Figure 8 shows a comparison of a PCI signal with a magnetic pick-up coil signal where there is a clear 2nd harmonic of the dominant Alfvén cascade from about 0.14 to 0.18 s at exactly twice the frequency and twice the slope of the AC in the PCI signal. Its amplitude is roughly 1/10th of the 1st harmonic, indicating the nonlinear character of these modes as expected by theory.^{26, 31} The 2nd harmonic is not visible on the magnetic pick-up coil signal suggesting that this mode has shorter wavelength and falls off more rapidly with radius than the 1st harmonic.

Just before the onset of the ACs there is sometimes also present a brief downward frequency sweeping mode from typically 1 MHz to 900 kHz visible on the magnetic pick-up coils, which is at twice the TAE frequency for $q=2$, indicating that it is an ellipticity induced Alfvén eigenmodes (EAEs)¹⁰ (Figure 9). This may indicate that the

q=2 surface is just entering the plasma at that time. Note that the EAE associated with q=2 ends just as the TAEs associated with q=2 appear at the top of the AC.

E. Alfvén eigenmode stability vs ICRF resonance position

To determine the effect of the ICRF resonance position on AE stability, an experiment was performed at constant RF frequency changing the toroidal field from shot-to-shot to move the hydrogen minority ICRF resonance position, R_{res} , from $R_{res}/R_{axis} = 0.9$ to $R_{res}/R_{axis} = 1.11$. Figure 10 shows the Fourier spectrograms of the Alfvén eigenmodes for three discharges with a) inboard, b) central, and c) outboard ICRF resonance positions. For the inboard resonance case, the usual Alfvén cascades and subsequent TAEs are not excited and only a couple of weak downward sweeping frequency modes are visible. The central resonance has the strongest drive for both the ACs and TAEs though the outboard resonance case also has relatively strong ACs and TAEs despite having substantially less average ICRF power.

Theory predicts that the drive for AEs should decrease as the resonance is moved toward the inboard side because the toroidal precession drift frequency decreases.^{31, 39} To attempt to isolate this physical effect, the central resonance case was modeled with the Nova-K code including finite orbit width and finite Larmor radius effects⁴⁰ to calculate the trapped particle contribution to the growth rate of AEs as a function of ICRF resonance position. The fast particle distribution function in Nova-K goes as

$f \propto \exp[-E/E_H - (p - R_{res}/R_{axis})^2 / (dR/R_{axis})^2]$, where $E = \frac{1}{2}mv^2$, E_H is the input

fast ion energy, $p = \mu B_{axis}/E$, $\mu = \frac{1}{2}mv_{\perp}^2/B$ is the magnetic moment of the fast ions, R_{axis}

is the major radius of the magnetic axis, and dR is the half width of the RF power

deposition. The fast particle profiles were calculated with TRANSP/FPPRF at $t=0.122$ s

at the top of one of the ACs and R_{res}/R_{axis} was varied from 0.8 to 1.14 keeping everything else fixed. The q profile was assumed to have slightly reversed shear with $q_0 = 2.11$ and $q_{min} = 2.06$ at $r/a = 0.4$, then smoothly matching the equilibrium edge q value. An unstable $n=1$ mode was found with a frequency of 342 kHz, which is close to the measured AE frequency of 360 kHz. Figure 11a shows first the calculated trapped particle growth rate including collisional, radiative, and Landau damping as a function of E_H . The growth rate peaks at a fast ion energy of about 160 keV, which is the same value that TRANSP/FPPRF calculations give at this time. The decay in the growth rate with increasing fast ion energy is due to averaging out of the mode over larger and larger Larmor radii. Note that if a Stix distribution were used, there would be more low energy particles and a substantially higher asymptotic energy for the high energy particles, both of which would tend to lower the calculated growth rate. Figure 11b shows the calculated growth rate for this mode as a function of R_{res}/R_{axis} at the fast ion energy of 160 keV. The growth rate for the inboard resonance at $R_{res}/R_{axis} = 0.9$ is substantially lower than for either the central resonance case or the outboard resonance case at $R_{res}/R_{axis} = 1.11$, in qualitative agreement with the experiment. This comparison, however, assumes that the damping rate does not change substantially from the inboard to the outboard RF resonance. More quantitative agreement for the different discharges would require measurements of the fast ion distribution.

V. Conclusions

Stable and unstable Alfvén eigenmodes are measured on Alcator C-Mod with equilibrated ion and electron temperatures at the same densities and toroidal fields and in

the same toroidal mode range as expected in ITER. Moderate n from 4 to 14 stable TAE resonances have been excited for the first time and initial scaling of their damping rates has been measured. The measured damping rate for this range of moderate n stable TAEs does not show any clear dependence on the edge magnetic shear, in contrast to the increasing damping rates with increasing shear found on JET for low $n \leq 2$ modes with monotonic q profiles.¹⁴ While these results may indicate that the damping of low n modes is dominated by the edge and that of moderate n modes is not, the results could be masked by a change in damping due to changing n numbers during the scan. More shape scan experiments measuring the TAE damping rates are required to better define the damping rate dependence on shape and toroidal mode number.

During sawtooth stabilization with ICRF, multiple n fast particle driven modes coalesce to a single frequency and mode just before the sawtooth collapse. Nova-K modeling finds only stable modes under these conditions, perhaps indicating they are energetic particle driven modes that are not modeled by the code.

Alfvén cascades during the current rise with strong ICRF heating have been used to constrain the q profile indicating a very flat shear profile across the plasma core. A second harmonic of the Alfvén cascades is sometimes observed on PCI measurements in the core of the plasma with $1/10^{\text{th}}$ the amplitude of the first harmonic indicating that these modes are nonlinear, as expected by theory. Through a toroidal field scan at fixed ICRF frequency, the RF resonance was scanned from inboard to outboard and the Alfvén cascades and TAEs were found to be more stable for an inboard resonance than for a central or outboard resonance. This is expected by theory since the toroidal precession drift frequency slows down for an inboard resonance. The Nova-K calculated growth

rate as a function of the RF resonance position is in qualitative agreement with the experiment assuming little change in the damping rate.

ACKNOWLEDGEMENTS

We would like to thank the Alcator C-Mod team for all their hard work keeping the tokamak and its diagnostics running to acquire the data used in these experiments. We would also like to thank F. Zonca for valuable discussions. This work is supported by the U. S. Department of Energy Contract DE-FC02-99ER54512.

- ¹K. L. Wong, R. J. Fonck, S. F. Paul, *et al*, Phys. Rev. Lett. **66**, 1874 (1991).
- ²W. W. Heidbrink, E. J. Strait, E. Doyle, and R. Snider, Nucl. Fusion **31**, 1635 (1991).
- ³M. Saigusa, H. Kimura, S. Moriyama, Y. Neyatani, T. Fujii, Y. Koide, T. Kondoh, M. Sato, M. Nemoto, Y. Kamada and JT-60 Team, Plasma Phys. Cont. Fus. **37**, 295 (1995).
- ⁴A. Fasoli, J.B. Lister, S.E. Sharapov, *et al*, Nucl. Fusion **35**, 1485 (1995).
- ⁵A. Weller, D. A. Spong, R. Jaenicke, A. Lazaros, F. P. Penningfield, S. Sattler, W7-AS Team, and NBI Group, Phys. Rev. Lett. **72**, 1220 (1994).
- ⁶N. N. Gorelenkov, S. Bernabei, C. Z. Cheng, *et al*, Nucl. Fusion **40**, 1311 (2000).
- ⁷M. N. Rosenbluth and P. H. Rutherford, Phys. Rev. Lett. **34**, 1428 (1975).
- ⁸C. Z. Cheng, L. Chen, and M. S. Chance, Ann. Phys (N.Y.) **161**, 21 (1985).
- ⁹G. Y. Fu, and J. W. Van Dam, Phys. Fluids B **1**, 1949 (1989).
- ¹⁰R. Betti and J. P. Freidberg, Phys. Fluids B **4**, 1465 (1992).
- ¹¹Fulvio Zonca and Liu Chen, Phys. Fluids B **5**, 3668 (1993).
- ¹²G. Y. Fu, C. Z. Cheng, R. Budny, Z. Chang, D. S. Darrow, E. Fredrickson, E. Mazzucato, R. Nazikian, K. L. Wong, and S. Zweben, Phys. Plasmas **3**, 4036 (1996).
- ¹³A. Fasoli, D. Borba, G. Bosia, D. J. Campbell, et al, Phys. Rev. Lett. **75**, 645 (1995).
- ¹⁴D. Testa, A. Fasoli, Nucl. Fus. **41**, 809 (2001).
- ¹⁵A. Fasoli, D. Testa, S. Sharapov, H. L. Berk, B. Breizman, et al, Plasma Phys. Cont. Fus. **44**, B159 (2002).
- ¹⁶C. E. Kieras and J A Tataronis, J. Plasma Phys. **28**, 395 (1982).
- ¹⁷J. A. Snipes, D. Schmittiel, A. Fasoli, R. S. Granetz, and R. R. Parker, Plasma Phys. Cont. Fus. **46**, 611 (2004).
- ¹⁸M. Saigusa *et al* Plasma Phys. Cont. Fus. **40**, 1647 (1998).
- ¹⁹S. Bernabei *et al* Phys. Rev. Lett. **84**, 1212 (2000).
- ²⁰S. Bernabei *et al* Nucl. Fus. **41**, 513 (2001).
- ²¹Francesco Porcelli, Plasma Phys. Cont. Fus. **33**, 1601 (1991).
- ²²H. Kimura, Y. Kusama, M. Saigusa, G. J. Kramer, K. Tobita, et al, Nucl. Fus. **38**, 1303 (1998).
- ²³S. E. Sharapov, B. Alper, H. L. Berk, D. N. Borba, B. N. Breizman, et al, Phys. Plasmas **9**, 2027 (2002).
- ²⁴J. A. Snipes, A. Fasoli, P. Bonoli, S. Migliuolo, M. Porkolab, et al, Plasma Phys. Cont. Fus. **42**, 381 (2000).
- ²⁵R. Nazikian, G. J. Kramer, C. Z. Cheng, N. N. Gorelenkov, H. L. Berk, and S. E. Sharapov, Phys. Rev. Lett. **91**, 125003 (2003).
- ²⁶H. L. Berk, D. N. Borba, B. N. Breizman, S. D. Pinches, and S. E. Sharapov, Phys. Rev. Lett. **87**, 185002 (2001).
- ²⁷A.B.Mikhailovskii, G. T. A. Huysmans, W. O. K. Kerner, and S. E. Sharapov, Plasma Phys Rep **23**, 844 (1997).
- ²⁸S. Poedts, *et al* Plasma Phys Cont Fus **34**, 1397 (1992).
- ²⁹G. J. Kramer, S. E. Sharapov, R. Nazikian, N. N. Gorelenkov, and R. V. Budny, Phys. Rev. Lett **92**, 015001 (2004).
- ³⁰G. Y. Fu and C. Z. Cheng, Phys. Fluids B **4**, 3722 (1992).
- ³¹F Zonca, S. Briguglio, L. Chen, S. Dettrick, G. Fogaccia, D. Testa, and G. Vlad, Phys Plasmas **9**, 4939 (2002).
- ³²G. J. Kramer, C. Z. Cheng, G. Y. Fu, *et al*, Phys. Rev. Lett. **83**, 2961 (1999).

- ³³A. Mazurenko, M. Porkolab, D. Mossessian, J. A. Snipes, X. Q. Xu, and W. M. Nevins, Phys. Rev. Lett. **89**, 225004 (2002).
- ³⁴S. E. Sharapov, B. Alper, J. Fessey, et al, Phys. Rev. Lett. **93**, 165001 (2004).
- ³⁵A. Mazurenko, Ph.D. thesis, Massachusetts Institute of Technology, Cambridge, MA, 2001.
- ³⁶G. W. Hammett, Ph.D. thesis, Princeton University, Princeton, NJ, 1986.
- ³⁷M. Brambilla, Plasma Phys. Cont. Fusion **41**, 1 (1999).
- ³⁸T. H. Stix, Nucl. Fus. **15**, 737 (1975).
- ³⁹R B White, *Theory of Tokamak Plasmas* (North-Holland, New York, 1989), p. 78.
- ⁴⁰N. N. Gorelenkov, C. Z. Cheng, and G. Y. Fu, Phys. Plasmas **6**, 2802 (1999).

Figure Captions

Figure 1. Fourier spectrogram and time average of a poloidal field pick-up coil signal showing two clear resonances during excitation of the upper active MHD antenna at constant frequency (409 kHz) as the TAE frequency in the plasma is ramped through the active frequency twice by ramping the toroidal field down and back up during the discharge.

Figure 2. Fourier spectrogram of a poloidal field pick-up coil signal during programmed frequency sweeping of the active MHD antenna together with the time average of the perturbed poloidal field. Weak resonances are found as the active frequency passes through the TAE frequency in the plasma calculated at the $q=1.5$ surface.

Figure 3. The measured TAE damping rate as a function of plasma elongation and magnetic shear at the 95% flux surface for a range of moderate n modes from $4 \leq n < 14$.

Figure 4. a) Fourier spectrogram of an edge poloidal field pick-up coil signal showing multiple Alfvén eigenmodes during sawtooth stabilization together with the electron

temperature measured from ECE and the ICRF power; b) the toroidal mode spectrum showing the n number begin at n=10 and decrease to n=4 just before the sawtooth collapse.

Figure 5. Fourier spectrograms of an edge poloidal field pick-up coil signal and a core PCI signal showing Alfvén cascades with steeper slopes in the core than at the edge.

Figure 6. MISHKA modeling of the evolution of the minimum q value based on the frequency evolution of the Alfvén cascades of Figure 4 together with the modeled q profile at t=0.12 s.

Figure 7. a) TRANSP/FPPRF calculated fast hydrogen ion energy as a function of time during the Alfvén eigenmodes of Figure 4. b) Radial profiles of the fast ion energy and the RF power deposition at 0.2 s.

Figure 8. a) Fourier spectrogram of phase contrast imaging density fluctuations during the current rise showing a clear 2nd harmonic of the dominant Alfvén cascade. b) Fourier spectrogram of a poloidal field pick-up coil signal showing that the 2nd harmonic is not visible, though other modes at about twice the TAE frequency are observed.

Figure 9. Fourier spectrogram of a poloidal field pick-up coil signal showing the appearance of an ellipticity induced Alfvén eigenmode (EAE) associated with q=2 just before an Alfvén cascade. Curves are shown for the approximate center of the gap

frequencies for the EAE ($f_{\text{EAE}} = v_A/(2\pi qR)$) and TAE ($f_{\text{TAE}} = v_A/(4\pi qR)$) at $q=2$ using the core line averaged electron density and toroidal field on axis in v_A .

Figure 10. Fourier spectrograms of a magnetic pick-up coil and PCI channel showing Alfvén eigenmodes for a) inboard ($R_{\text{res}}/R_{\text{axis}} = 0.9$), b) central ($R_{\text{res}}/R_{\text{axis}} = 1.02$), and c) outboard ($R_{\text{res}}/R_{\text{axis}} = 1.11$) ICRF resonance positions. The Alfvén cascades and TAEs are clearly more unstable for central and outboard resonance positions rather than for the inboard resonance position.

Figure 11. Nova-K modeling of the growth rate for an $n=1$ mode in the central resonance case from Figure 10 b) as a function of (a) the fast particle energy, E_H and (b) the ICRF resonance position, keeping all other parameters fixed.

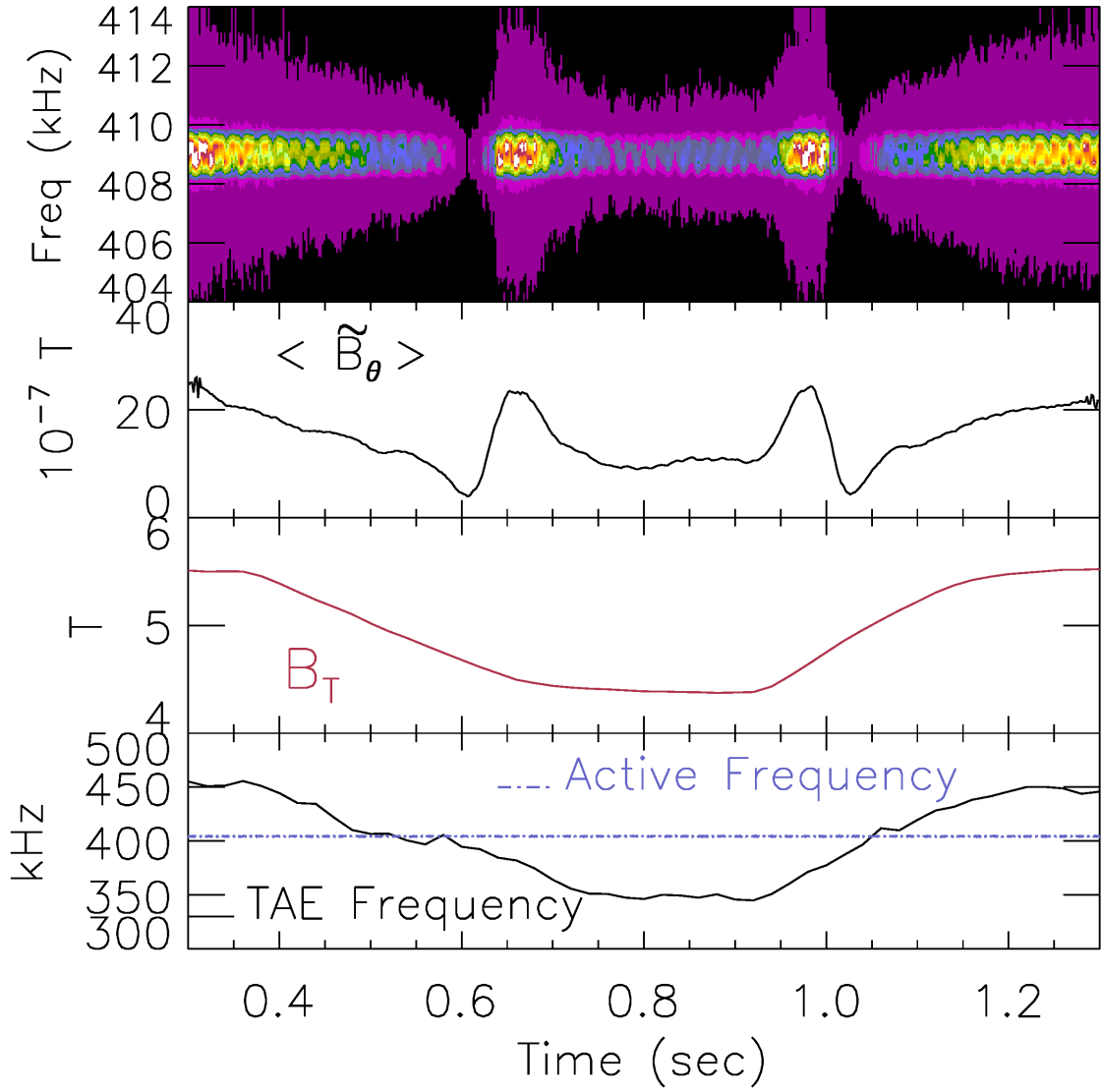


Figure 1

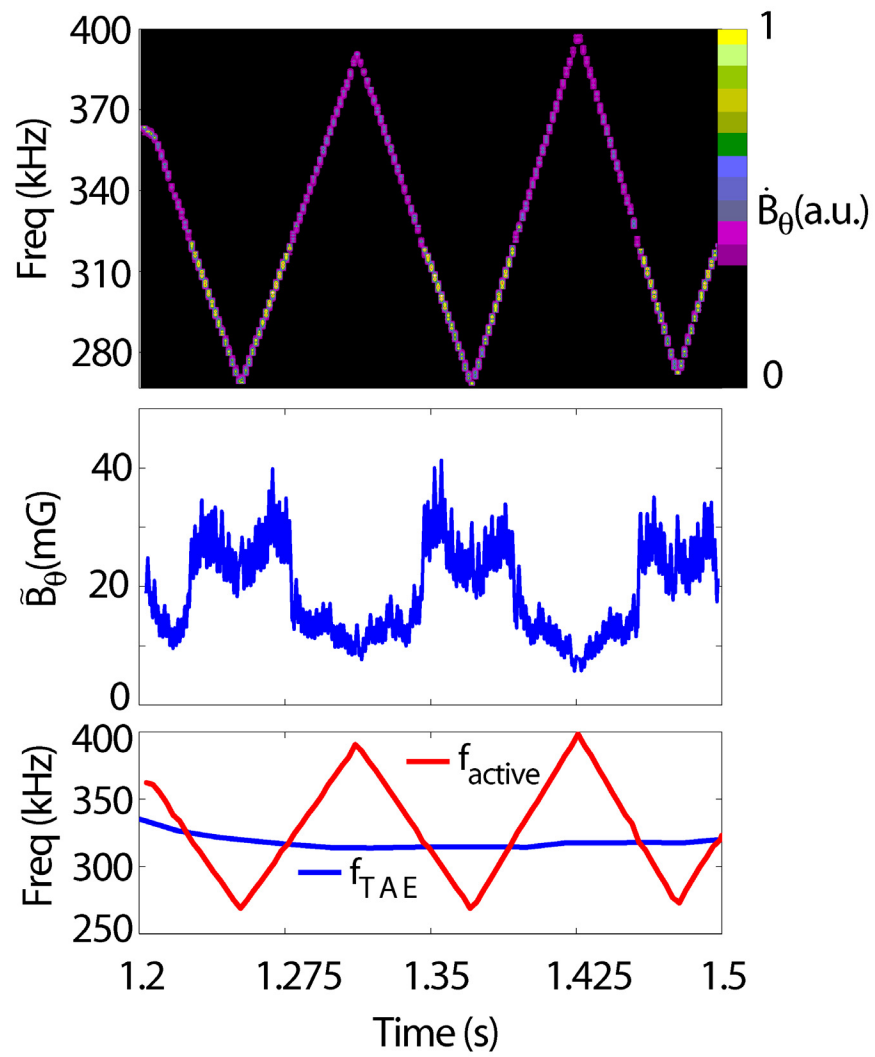


Figure 2

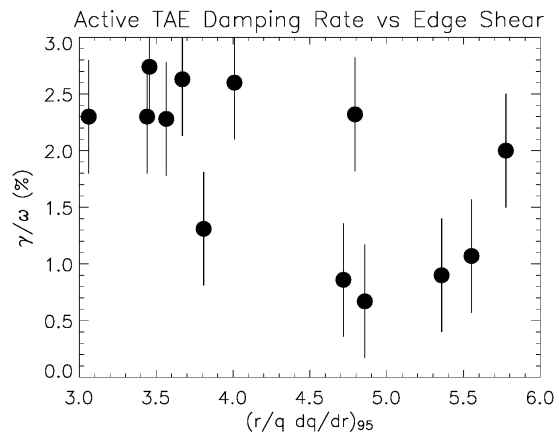
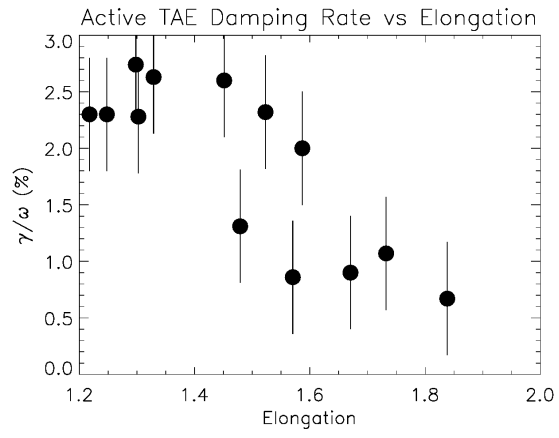


Figure 3

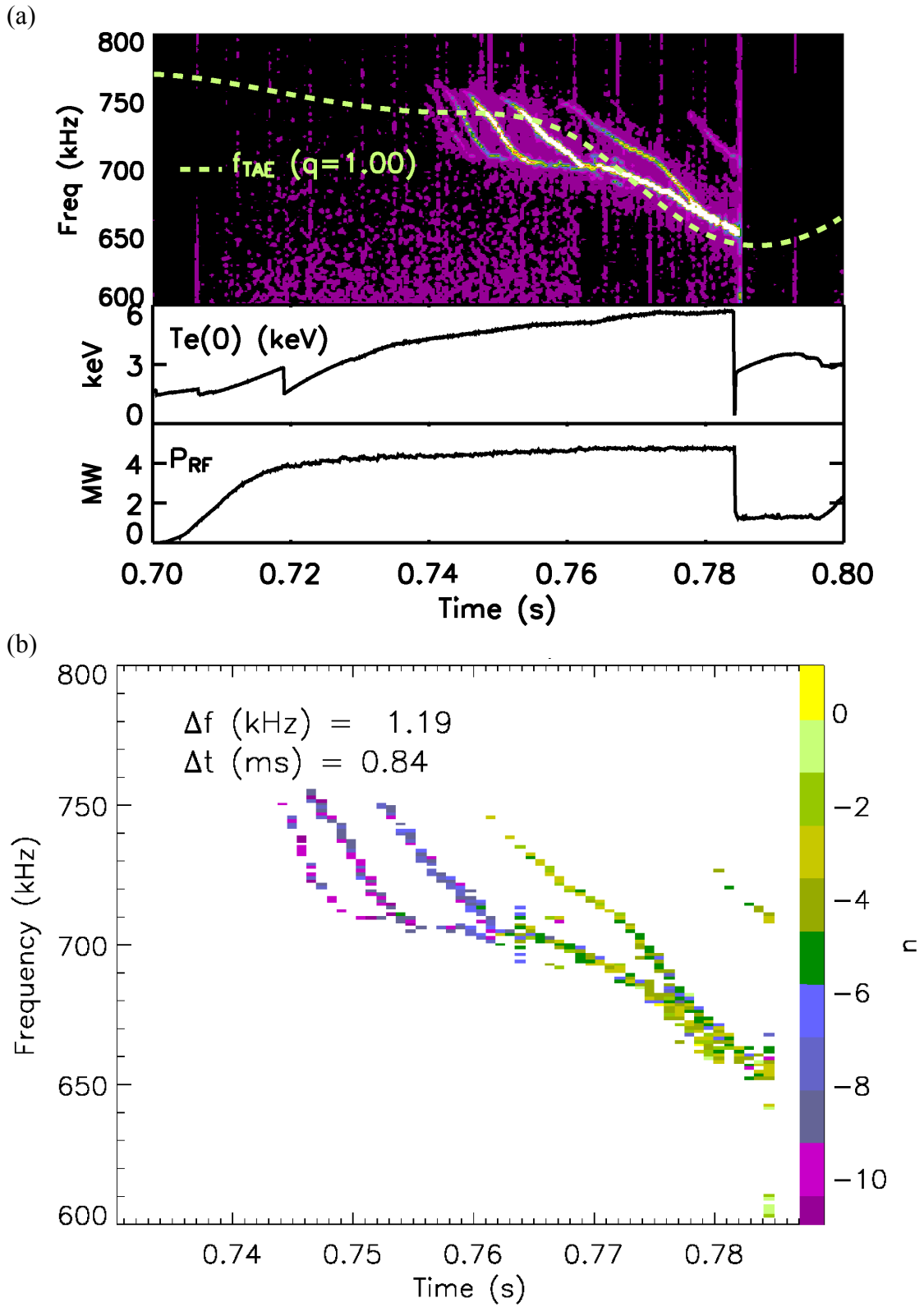


Figure 4

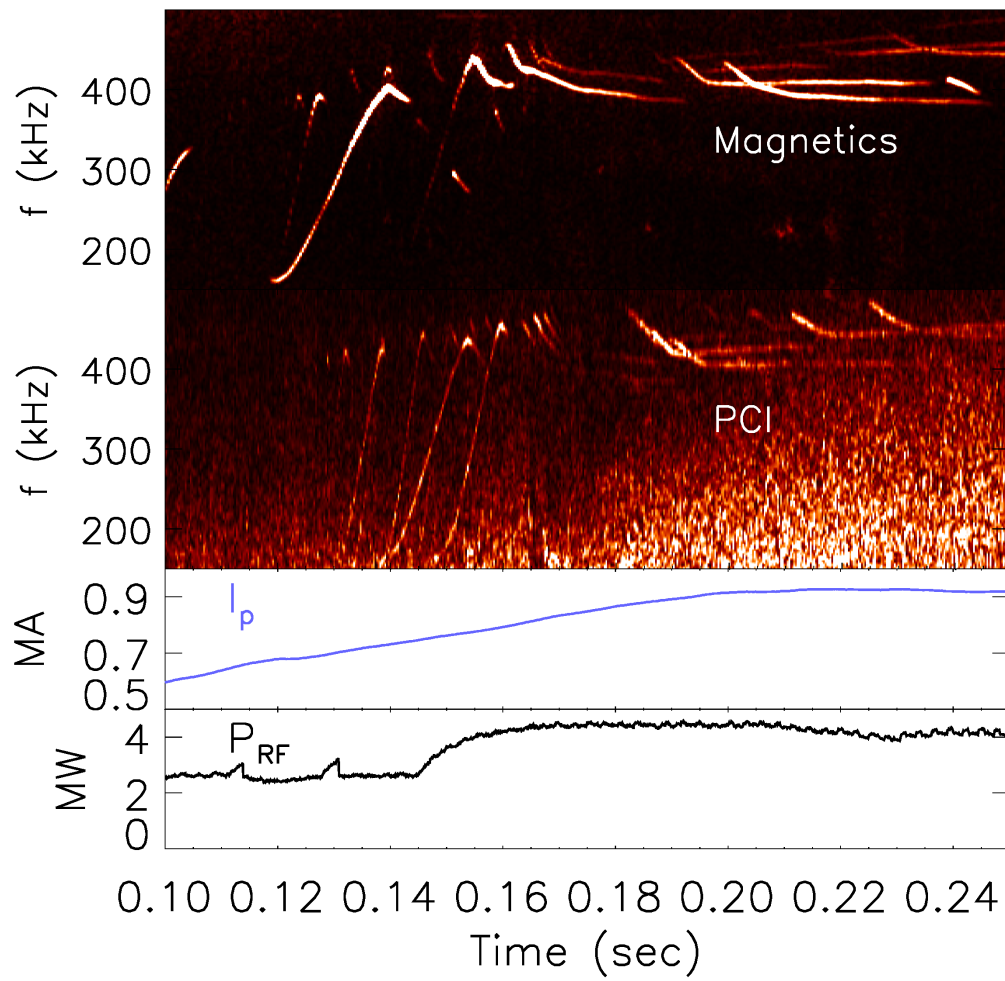


Figure 5

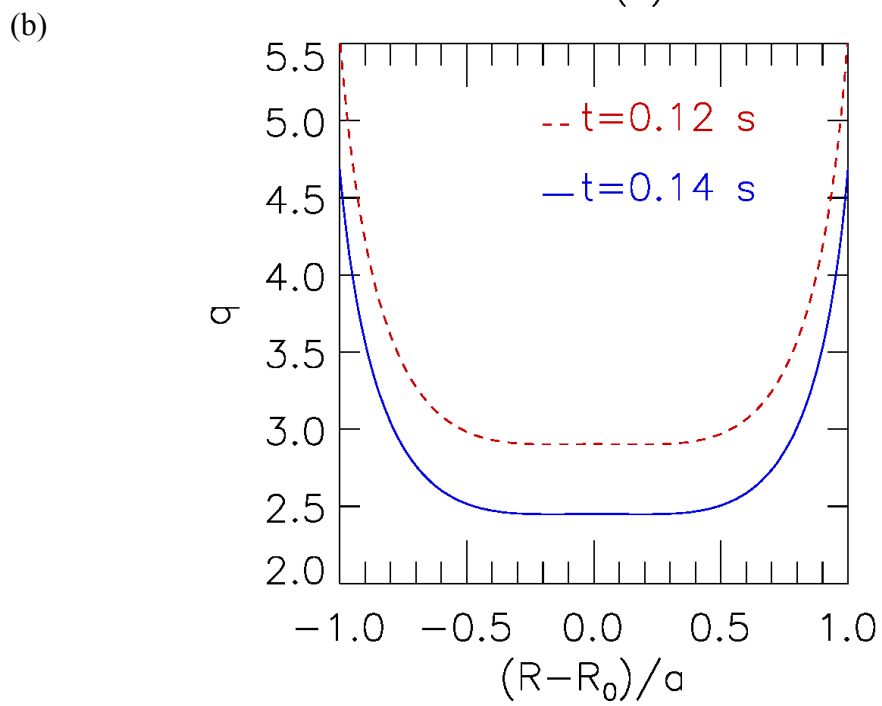
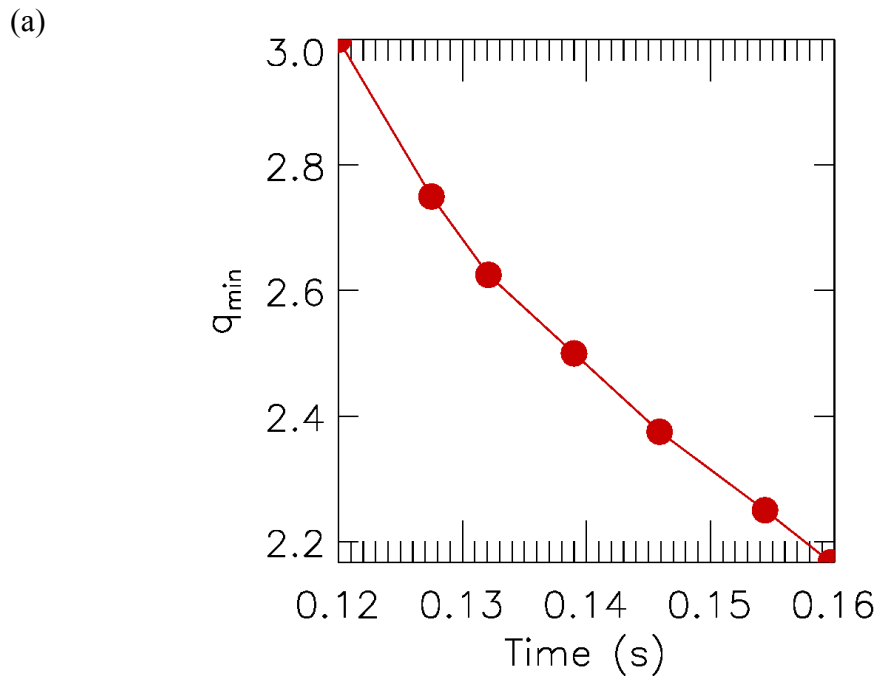
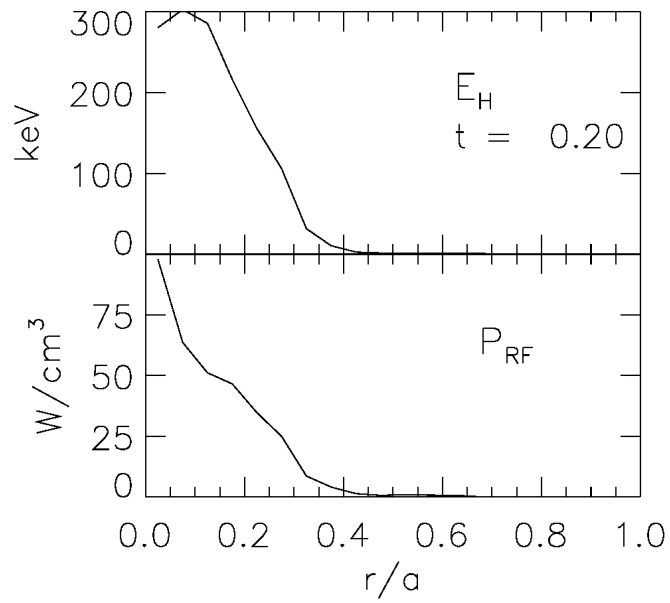
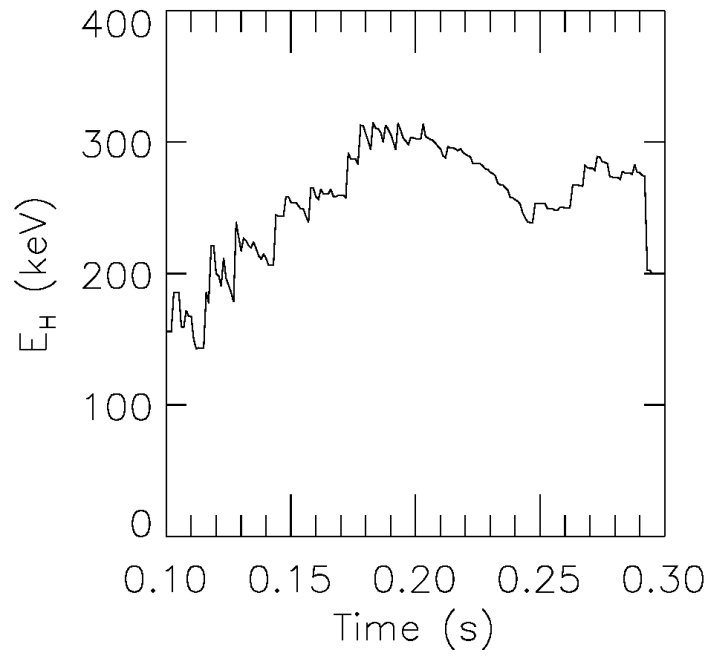


Figure 6

(a)



(b)

Figure 7

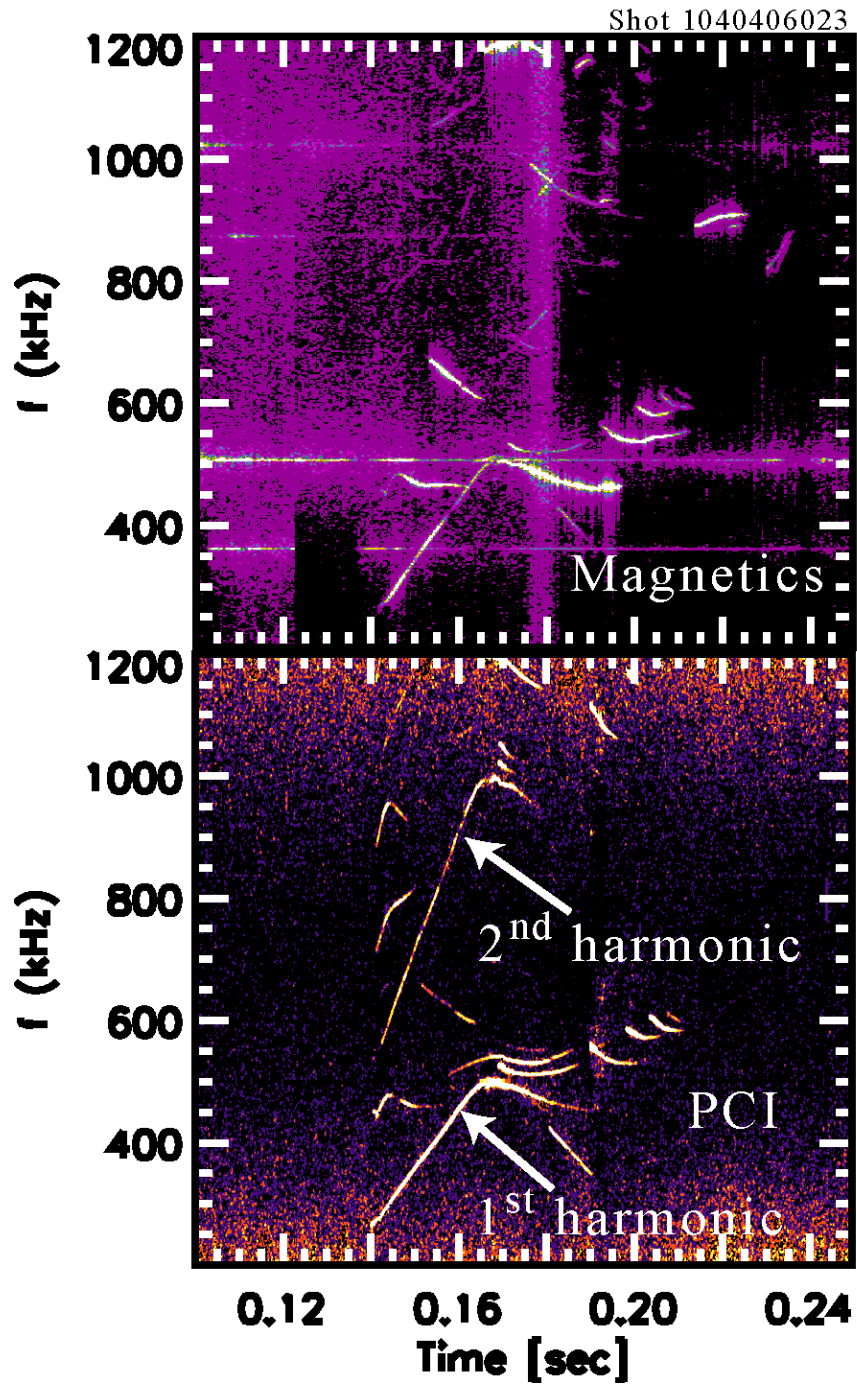


Figure 8

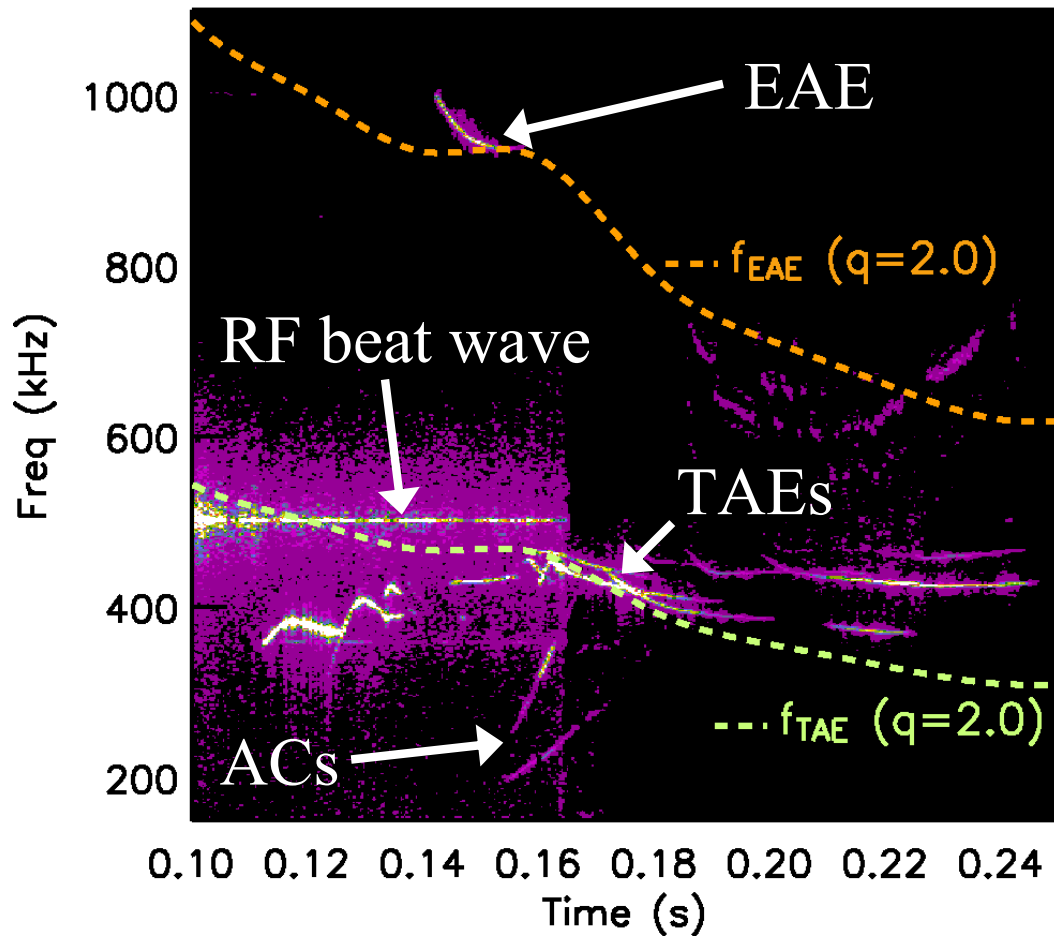


Figure 9

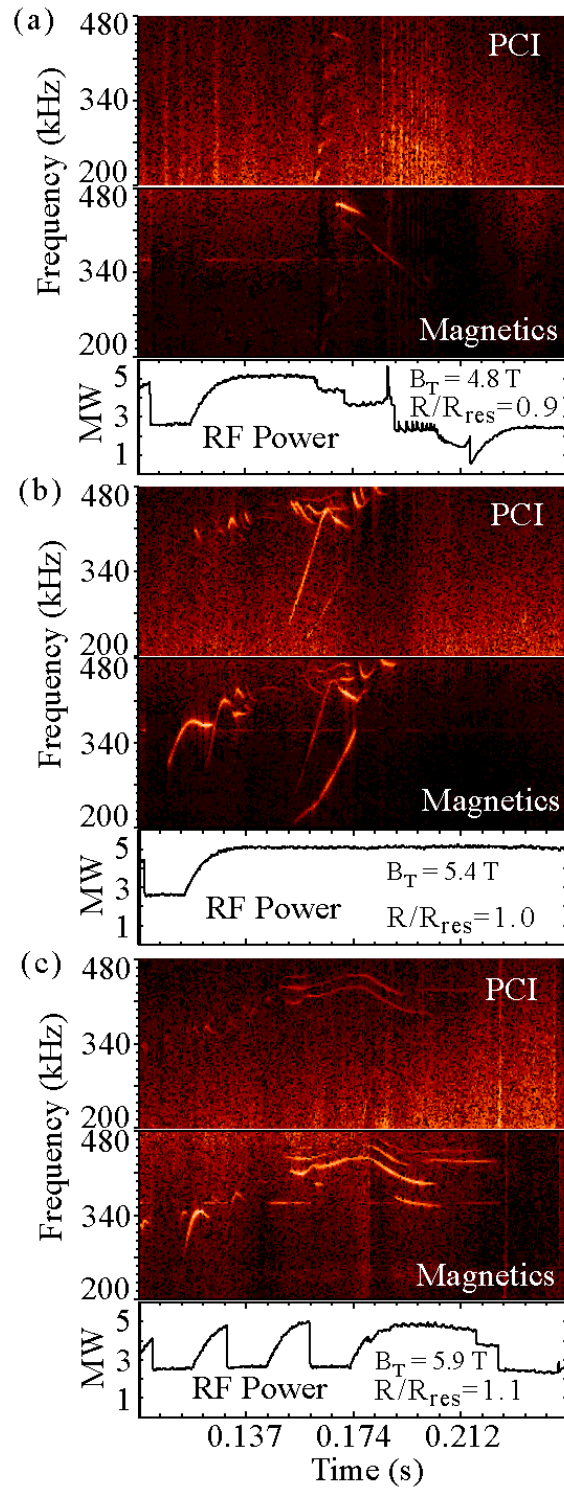
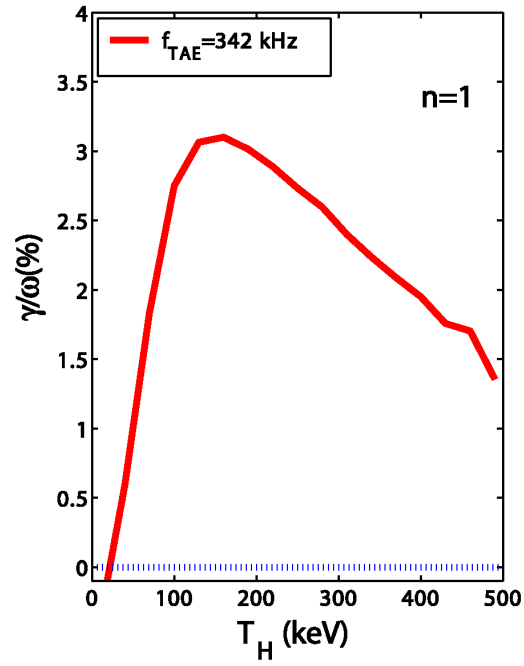
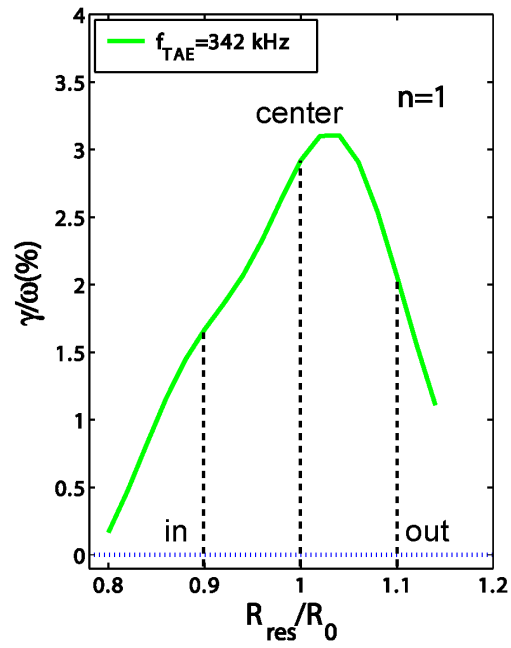


Figure 10



(a)



(b)

Figure 11